Physics Mechanisms of Toroidal Rotation Profile and Properties of Momentum Transport in JT-60U

M. Yoshida, Y. Kamada, H. Takenaga, Y. Sakamoto, H. Urano,
N. Oyama, G. Matsunaga, and the JT-60 Team

Japan Atomic Energy Agency, 801-1, Mukoyama, Naka 311-0193, Japan

The roles of the elements determining the toroidal rotation velocity (V_t) profile, i.e. the momentum transport, the external momentum input, and the intrinsic rotation are found by the transient momentum transport analysis. The perturbation techniques enable us to evaluate the momentum diffusivity (χ_ϕ) and the convection velocity (V_{conv}), and to calculate V_t profiles driven by external torque input by neutral beams (NBs). The measured V_t profiles at low heating power are almost reproduced by χ_ϕ and V_{conv}. At higher heating power, the CTR directed (anti-parallel to the plasma current, I_p) intrinsic rotation, which is locally determined by the local pressure gradient is observed in the core region. This rotation increases with increasing the pressure gradient in CO and CTR rotating L-mode plasmas. Concerning the momentum transport, χ_ϕ increases with increasing heating power, and decreases with increasing I_p. In the H-mode plasmas, χ_ϕ is smaller than that in the L-mode under similar experimental conditions. It is found that χ_ϕ separated from non-diffusive term increases with increasing the heat diffusivity (χ_i), and $-V_{conv}$ increases with increasing χ_ϕ in H-mode plasmas.

Keywords: toroidal rotation velocity, intrinsic rotation, momentum transport, L-mode, H-mode.

1. Introduction

The Burning plasma is the self-regulating system, where the pressure, rotation, and current profiles are strongly linked to each other [1]. The JT-60 project has addressed major physics issues towards the understanding and the operation of the burning steady-state plasmas, and promoted an integrated research project focusing on the rotation. In many present-day tokamak experiments, the toroidal rotation velocity (V_t) is driven by external momentum input from neutral beam (NB) injection. However, in future burning plasma experiments, the external momentum input from the auxiliary heating is expected to be small. Intrinsic toroidal plasma rotations generated by the plasma itself have recently become the subject of intense interest and investigation in the magnetically confined tokamak plasma research, since such an intrinsic rotation could dominate the total plasma rotation in future devices [2]. Therefore, the critical importance of understanding the physical mechanisms determining the V_t profile including the intrinsic rotation, and controlling V_t profile has been increasingly recognized for next step devices.

It is now widely recognized that the rotation and its radial shear play essential roles in determining magnetohydrodynamic stability at a high plasma pressure, such as the stabilization of the resistive-wall mode [3, 4], and in the suppression of turbulence leading to enhanced confinement, such as the transport barrier formation [5, 6]. However, the mechanism determining rotation profile is not understood well. Because the V_t profiles are determined by various mechanisms. The worldwide progress in understanding the physics of momentum transport and rotation has been made experimentally [7-12] and theoretically [13-15]. As for the elements determining the V_t, characteristics of momentum transport which consists of diffusive (the toroidal momentum diffusivity, χ_ϕ) and non-diffusive (the convection velocity, V_{conv}) terms [7, 12], the external momentum input and the intrinsic rotation [8-11] have been reported individually. However, the understanding of rotation mechanisms with integrating all of the terms (the momentum transport, the external momentum input and the intrinsic rotation) remains an open issue despite its urgency towards the next step devices. This is due mainly to an experimental difficulty in evaluating the diffusive term of the momentum transport, the non-diffusive term of that and the intrinsic rotation separately.

In order to address this issue, we have applied the perturbation techniques developed in our recent works [7,

author's e-mail: journal@jspf.or.jp

12], which enable us to evaluate χ_ϕ and V_{conv} separately. As a novel momentum source, fast ion losses due to the toroidal field ripple, which locally induce a toroidal rotation in the direction antiparallel to the plasma current, i.e. the counter (CTR) direction in the peripheral region through the formation of an inward electric field have been used [7]. This momentum source is found by a beam perturbation experiment and orbit following Monte Carlo (OFMC) code [16]. The effects of the ripple loss of fast ions on the toroidal rotation are also investigated by using data with and without ferritic steel tiles (FSTs) [16]. The characteristics of the χ_ϕ and the V_{conv}, and the correlations between χ_ϕ, V_{conv} and χ_i are investigated by I_p and heating power scans in L- and H-mode plasmas. We have separately identified the roles of the momentum transport and the intrinsic rotation on V_t profiles in the CO (in the direction to the plasma current, I_p), and CTR rotating L-mode plasmas. In this paper, negative sign of V_t designates CTR-directed rotation and positive sign of V_t CO-directed rotation, and the momentum balance equation is solved using a cylindrical model for toroidal momentum with flux surface averaged parameters.

2. Neutral beams in JT-60U

In JT-60U [17], NBs of various injection geometries are installed. They consist of; two tangential beams directing the same direction as that of the plasma current (CO-NBs), two tangential beams directing opposite to the plasma current (CTR-NBs) and seven near perpendicular beams as shown in Fig. 1(a). The injection angle of tangential beams is 36 degree and that of near-perpendicular neutral beam (PERP-NB) is 75 degree with respect to the magnetic axis. The deuterium beam acceleration energy is about 85 keV, and the input power per injected unit is about 2 MW. The plasma rotation in the toroidal direction is varied using a combination of these NBs. In addition such a direction, one of each tangential beams in the same direction is almost on-axis deposition and the other is off-axis deposition, four of PERP-NBs are almost on-axis deposition and the others are off-axis deposition as shown in Fig. 1(b).

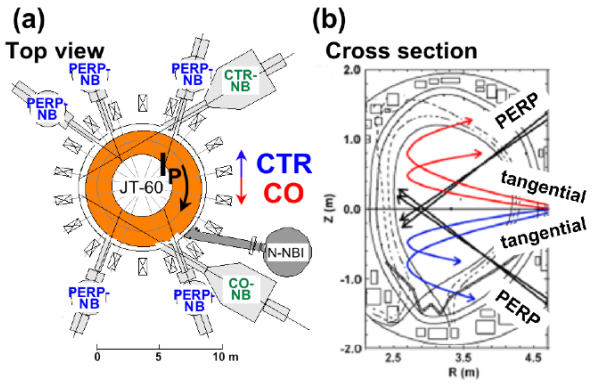

Fig.1 (a) Neutral beam (NB) system on JT-60U (b) A poloidal cross-section with NB trajectories.

3. Driving source of CTR rotation

In JT-60U, CTR rotation is observed with PERP-NB injections in the case with large ripple loss condition. In this section, the effects of the ripple loss of fast ions and the location of the driving source of CTR rotation are investigated in an L-mode plasma.

The relation between V_t in the peripheral region (r/a~0.9) and the ripple loss power is investigated by NB power and the toroidal field ripple (with and without FSTs) scans, as shown in Fig. 2(a). In this data set, I_P, the toroidal magnetic field (B_T), the plasma volume (Vol.), and the line averaged electron density ($\bar{n}_e$) are kept almost constant (I_p=1.15 MA, B_T=2.6 T, the safety factor at 95% flux surface, q_{95}~4.1, Vol.~65 m^3, $\bar{n}_e \sim 1.5-2\times10^{19}\,m^{-3}$). Each arrow indicates the change in V_t by installing FSTs under the condition of almost same absorbed power (solid arrow: P_{ABS}~1.4-1.8 MW, dotted arrow: P_{ABS}~2.8-3 MW). As shown in Fig. 2(a), it is recognized that the systematic dependence of CTR rotation on the ripple loss of fast ions can be obtained by using data with and without FSTs.

In order to confirm the location of the driving source of CTR rotation, beam perturbation techniques [7] are

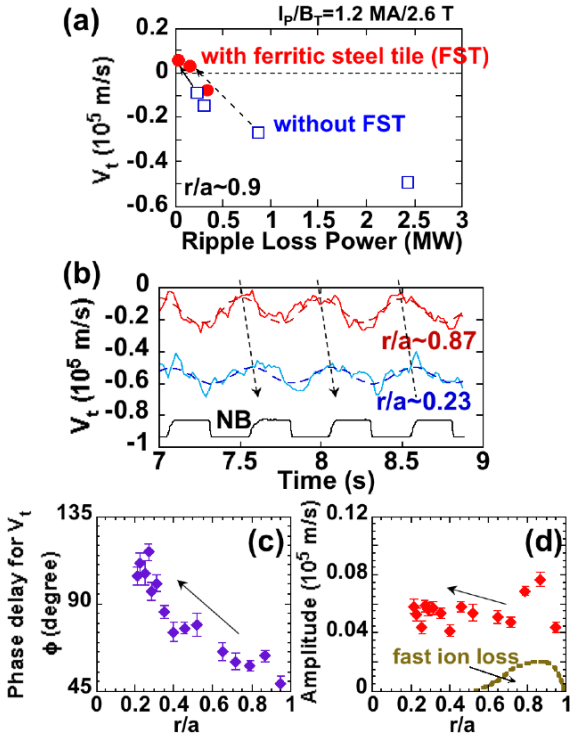

Fig.2 (a) V_t dependence on the ripple loss power. (b) Response of V_t to modulated beams. Profiles of (c) phase delay, (d) modulated amplitude, fast ion loss.

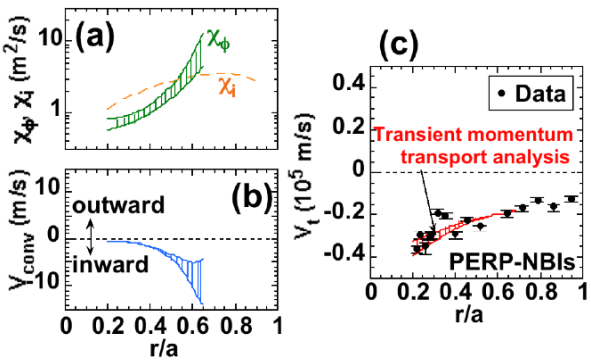

Fig.3 Profiles of (a) the toroidal momentum diffusivity (χ_ϕ), (d) the convection velocity (V_{conv}), and (c) V_t from calculation and measurements.

applied in an L-mode plasma. In this experiment, the plasma with low I_P (I_P=0.87 MA, B_T=3.8 T, q_{95}=8.2) and large volume (Vol.=72 m^3) was selected in order to enhance ripple losses. In order that the central region is free from direct external momentum input, off-axis PERP-NBs (the injected power P_{IN}=3.9 MW) are injected with a square wave modulation at 2 Hz into the discharge. As mentioned above, the injection angle of PERP-NBs is 75 degree with respect to the magnetic axis. For the purely PERP-NB injections (i.e. with no external momentum input), one unit of CO PERP-NB and that of CTR PERP-NB are injected simultaneously. Figure 2(b) shows the waveforms of modulated V_t at r/a=0.87 and 0.23 (solid lines), and the total injected power. Each trace is fitted to a sinusoidal function at the modulation frequency (dotted lines). The radial profiles of the phase delay ϕ and of the amplitude of the modulated part of the toroidal rotation velocity V_{t0} are shown in Figs. 2(c) and 2(d), respectively. The phase delay is taken from the start of NB injection. Using OFMC code [16], the profile of the prompt fast ion loss is also shown in Fig. 2(d). Large amplitude and small phase delay are recognized in the peripheral region (0.7<r/a<0.9), and this region agrees with the location at which fast ion losses take place. Therefore, we conclude the fast ion losses due to the toroidal field ripple induce CTR rotation in the edge region.

4. Evaluation of momentum transport coefficients

The toroidal momentum balance equations are written as

$$m_i \frac{\partial n_i V_t}{\partial t} = -\nabla \cdot M + S, \qquad (1)$$

$$M = -m_i \chi_\phi \frac{\partial n_i V_t}{\partial r} + m_i V_{conv} n_i V_t, \qquad (2)$$

where m_i, n_i, M and S are the ion mass, the ion density,

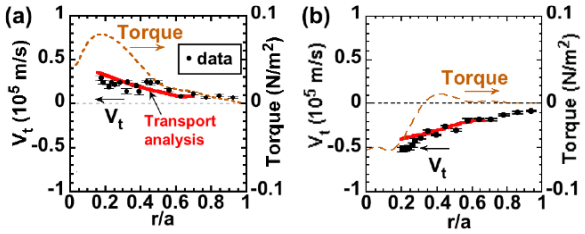

Fig.4 Data (solid circles) and reproduced V_t profile (solid lines) (a) with CO-NBI, (b) with CTR-NBI.

the toroidal momentum flux and the toroidal momentum source, respectively [7, 12]. In this paper, ions are defined as the main (deuterium) and impurity ions, assuming that the toroidal rotation velocity of the main ions is same as that of the carbon impurity ions, which is measured by the charge exchange recombination spectroscopy [18]. We can express the modulated n_iV_t assuming $n_i^c \tilde{V}_t >> \tilde{n}_i V_t^c$, $\tilde{n}_i \tilde{V}_t$ as follows (the validity of this assumption in this experiment is shown later),

$$\tilde{V}_t(r,t) = V_{t0}(r) sin\left(\omega t - \phi(r)\right), \qquad (3)$$

From equations (1)-(3), the time-independent solution of χ_ϕ and V_{conv} can be obtained [12].

Figures 3(a) and 3(b) show χ_ϕ and V_{conv} as evaluated from above mentioned modulation analysis (i.e. ϕ and V_{t0} profiles in Figs. 2(c) and 2(d)) assuming that the momentum source in the core region (0.2<r/a<0.65) is negligible (the momentum flux due to the modulated PERP-NBs, M on the left-hand side of equation (2) is one order of magnitude smaller than $-m_i\chi_\phi \partial n_i V_t/\partial r$ and $m_i V_{conv} n_i V_t$ at r/a~0.6). These transport coefficients in the region r/a>0.7 are not evaluated, because the driving source of CTR rotation is localized near the peripheral region as shown in Fig. 2(d).

The solid lines in Fig. 3(c) show V_t profiles calculated from equations (1) and (2) using transport coefficients in Figs. 3(a) and 3(b) with the boundary condition at r/a~0.65. Experimental data is also shown with solid circles. As shown in Fig. 3(c), V_t profile in the core region can be reproduced by momentum transport considering χ_ϕ and V_{conv}.

In Fig. 3(c), we compared the measured V_t profile to calculation from equations (1) and (2) using transport coefficients for a PERP-NBs injected L-mode plasma. We also treat the plasmas in which the external momentum source is injected, in order to investigate whether the toroidal rotation in the core region is dominated by the momentum transport with the coefficients. Experimental data (solid circles) in L-mode plasmas with one unit of CO tangential NB (I_P=1.2 MA, B_T=3.8 T, β_N=0.39, q_{95}=5.7 and $\bar{n}_e$=1.2x10^{19} m^{-3}) and that of CTR tangential NB (I_P=0.87 MA, B_T=3.8 T,

β_N=0.34, q_{95}=8.2 and $\bar{n}_e$=1.6x10^{19} m^{-3}) are shown in Figs. 4(a) and 4(b), respectively. In both plasmas, one unit of PERP-NB is injected for the CXRS measurements [18]. Toroidal momentum source (torque) density profiles (dashed line) are also shown. The solid lines show V_t profiles evaluated by the above-mentioned equations (1) and (2). In the both cases, the toroidal rotation profiles almost agree with calculations. The toroidal rotation profiles in the presence and absence of external torque have been explained by the momentum transport in the core region.

5. Characteristics of χ_ϕ and V_{conv}

Parameter dependences of the momentum transport coefficients (i.e. χ_ϕ and V_{conv}) evaluated above-mentioned method are shown in this section. Experiments have been carried out to investigate the momentum transport as the heating power is varied under otherwise similar conditions. As shown below, the degradation of momentum confinement with increasing heating power is observed similar to thermal confinement: the absorbed power range varied over the range 2.4 MW<P_{ABS}<10.7 MW. Over the entire power range, L-mode phase was maintained due to the high power threshold at the high B_T=3.8 T. The operation regimes in L-mode plasmas are β_N=0.39-1, ρ_{pol}*=0.03-0.05 and ν*=0.07-0.14. Here, β_N is the normalized β, ρ_{pol}* is the ion poloidal Larmor radius normalized to the minor radius, and ν* is the effective electron collision frequency normalized to the bounce frequency. As noted above, these L-mode plasmas satisfy L-mode scaling in JT-60U [19]. Other plasma parameters for this series of discharges were I_p=1.5 MA, q_{95}=4.2, δ=0.3 and Vol.=74 m^3. The profiles of χ_ϕ and V_{conv} during this heating power scan are shown in Figs. 5(a) and 5(b), respectively. The momentum diffusivity χ_ϕ increases systematically with increasing the heating power, and the shape of χ_ϕ is nearly identical. Non-diffusive inward flux exists and has maximum value at r/a~0.6. The dependences of χ_ϕ and V_{conv} at r/a=0.6 on absorbed power are shown in Fig. 5(c). The momentum diffusivity at r/a=0.6 roughly scaled linearly with heating power in this data set. The data in H-mode phase is also plotted in Fig. 5(c). The momentum diffusivity in the H-mode is smaller than in L-mode by factor of 2-3.

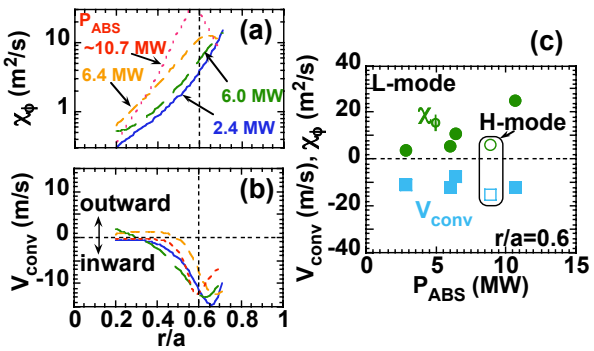

Fig.5 Profiles of (a) χ_ϕ and (b) V_{conv} during a heating power scan in L-mode plasmas. (c) Dependence of χ_ϕ and V_{conv} at r/a=0.6 on absorbed power.

6. Relation between χ_ϕ, χ_i and V_{conv}

In this section, the relations between χ_ϕ, χ_i, V_{conv} in H-mode plasmas are denoted by I_p and P_{ABS} scans.

After separating the diffusive and convective terms, the relation between χ_ϕ and χ_i is found for the fast time. Figures 6(a)-6(c) illustrate the radial profiles of χ_ϕ, V_{conv}, χ_i in a I_p scan, where B_T also varies so that q_{95}~4.3 is same value (I_p/B_T=1.2/2.8, 1.5/3.8, 1.8/4 MA/T). For these plasma discharges, two units of CO tangential NB and PERP-NBs are injected with P_{ABS}=7.2-8.9 MW. Other plasma parameters for this series of discharges were δ=0.35 and $\bar{n}_e$=2.0-2.5x10^{19} m^{-3}. The momentum diffusivity χ_ϕ decreases with increasing I_p over the whole radius. Also V_{conv} and χ_i decrease with increasing I_p. The dependences of the $1/\chi_\phi$ and $1/\chi_i$ at r/a=0.6 and the energy confinement time τ_E on I_p are also shown in Fig. 6(d). These coefficients are almost proportional to I_p, and the coefficients are similar value ($1/\chi_\phi$~0.12 I_p, $1/\chi_i$~0.14 I_p, τ_E~0.15 I_p).

The comparison of χ_ϕ and χ_i in the I_p scan is shown in Figs. 7(a) and 7(b). Figure 7(a) is the data from the profile data (0.25<r/a<0.6) shown in Figs. 6(a), and 6(b). The relation at fixed radius (r/a=0.5, 0.6) is shown in Fig. 7(b). A similar data set during the heating power scan is shown in Figs. 7(c) and 7(d), where two units of CO tangential NBs and PERP-NBs are injected at constant

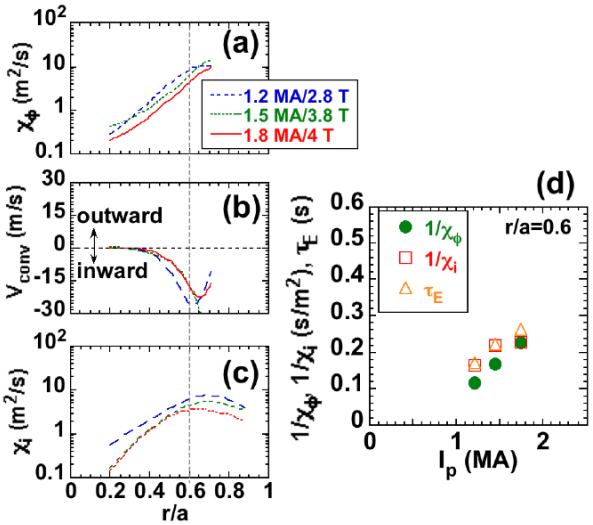

Fig 6 Profiles of (a) χ_ϕ, (b) V_{conv} and (c) χ_i during an I_p scan in H-mode plasmas. (c) Dependence of $1/\chi_\phi$ and $1/\chi_i$ at r/a=0.6 and τ_E on I_p.

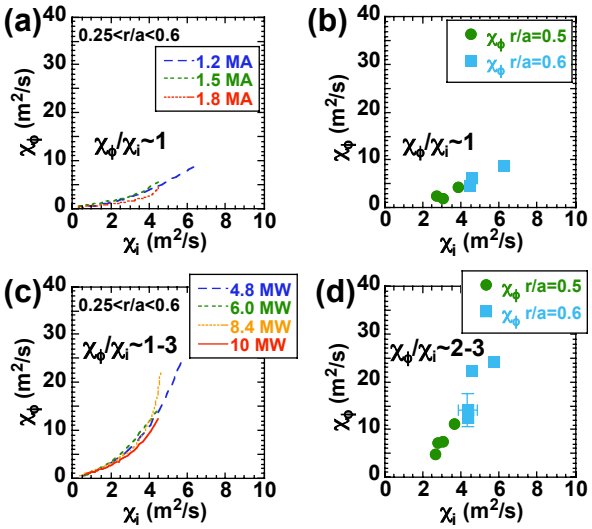

Fig.7 Relation of χ_ϕ and χ_i (a), (b) during the I_p scan, and (c), (d) during the heating power scan in H-mode plasmas. (a), (c) are the data from the profile, (b), (d) are the data at r/a=0.5, 0.6.

I_p=1.2 MA. Other plasma parameters for this series of discharges were δ=0.34 and $\bar{n}_e$=1.8-2.2x10^{19} m^{-3}. One can see that χ_ϕ increases with increasing χ_i. This tendency is observed over a wide range of radii for each discharge. In the case of the conventional steady-state analyses without considering V_{conv}, the evaluated χ_ϕ tended to be much smaller than χ_i. However, in this study, χ_ϕ is close to χ_i by analyzing both the diffusive and convective terms. This means that the momentum diffusivity is also anomalous in a similar level with the heat diffusivity.

We have also found the correlation between V_{conv} and χ_ϕ for the first time. Figures 8(a) and 8(b) show the correlation between -V_{conv} and χ_ϕ from the profile data in the region 0.25<r/a<0.6, and from the data at fixed radius (r/a=0.5, 0.6). The inward convection velocity (-V_{conv}) increases with increasing χ_ϕ over a wide range of radii for each discharge and at fixed radius in P_{ABS} and I_p scans. This finding of the correlation between χ_ϕ and V_{conv} can contribute to the understanding of the anomalous momentum transport.

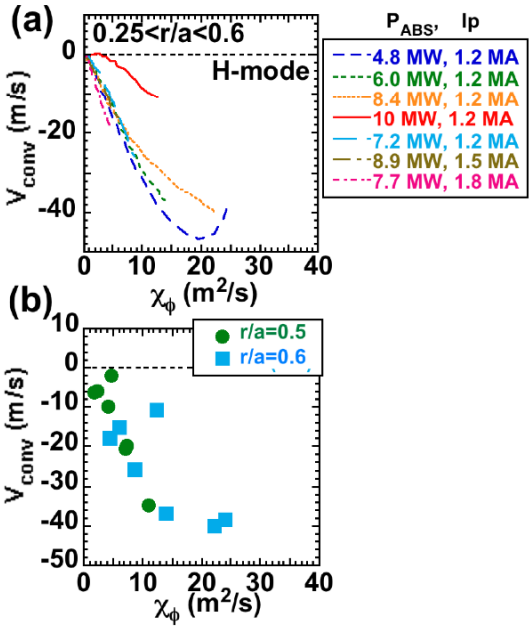

Fig.8 Correlation between V_{conv} and χ_ϕ (a) from the profile data for each discharge, and (b) at r/a=0.5, 0.6 in H-mode plasmas.

7. Intrinsic rotation

In section 4, the V_t profiles in the case with and without external momentum input can be almost reproduced by momentum transport calculations with χ_ϕ and V_{conv}. However, not all measured V_t can be explained with the momentum transport model including χ_ϕ and V_{conv}, the boundary condition of V_t, and the external momentum input by NBs. In this section, the characteristics of the V_t profiles, which cannot be explained with the momentum transport model, are investigated.

Figure 9(a) shows the radial profile of the measured V_t (open circles) in the case with a higher heating power P_{ABS}=11 MW L-mode plasma. The solid line in Fig. 9(a) shows the calculated V_t from the momentum transport equations using χ_ϕ and V_{conv} with the boundary condition (setting the measured V_t equal to the calculated one at r/a~0.65) [7]. Although the measured V_t agrees with the calculation in the region 0.45<r/a<0.65, the measured V_t deviates from the calculated one in the CTR-direction in the core region 0.2<r/a<0.45. These results mean that the measured V_t cannot be explained with the momentum transport model including momentum transport

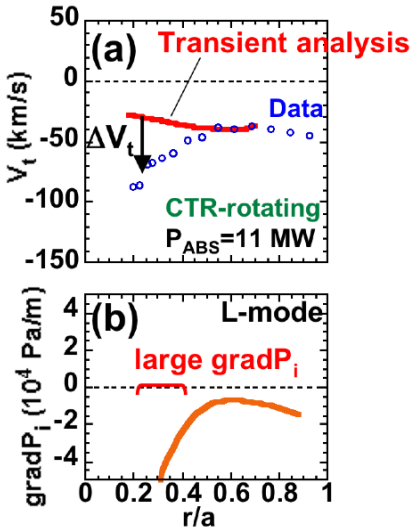

Fig.9 (a) Profiles of the measured V_t (open circles) and the calculated one (solid line), (b) and $gradP_i$ in the case of higher P_{ABS}=11 MW L-mode plasma.

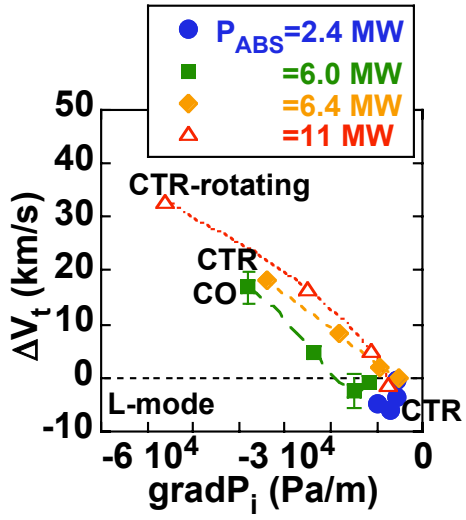

Fig.10 $-\Delta V_t$ is plotted against the $gradP_i$ in a heating power scan for L-mode (I_p=1.5 MA, B_T=3.8 T).

coefficients, the boundary condition of V_t, and the external momentum input by NBs. In such plasma, the large pressure gradient ($gradP_i$) is observed in the core region ($0.2<r/a<0.45$) as shown in Fig. 9(b).

In order to investigate the relation between the increase of CTR rotation and the $gradP_i$, the difference between the measured V_t and the calculated one, i.e. $\Delta V_t = V_t(measurement) - V_t(calculation) = intrinsic\ \ rotation$ in the region $0.3<r/a<0.6$ is plotted against the $gradP_i$ in the heating power scan in Fig. 10. The symbols denote ΔV_t at r/a=0.3, 0.4, 0.5 and 0.6. In these plasmas, the larger values of $gradP_i$ are obtained in the core region. As shown in Fig. 10, ΔV_t in L-mode plasmas grows with increasing $gradP_i$ in all cases. This tendency is almost the same, even the direction of the V_t is different (CO- and CTR-rotating plasmas), over a wide range of χ_ϕ which varies by about one order of magnitude radially (χ_ϕ~1-30 m^2/s) and by about a factor of three (χ_ϕ~1-3 m^2/s) (in the heating power scan) at fixed radius (r/a~0.4). These results indicate $gradP_i$ affects the intrinsic rotation even in L-mode plasmas, and the local $gradP_i$ affects the local value of the intrinsic rotation. This good correlation between the local intrinsic rotation velocity and the local $gradP_i$ indicates that the $gradP_i$ appears to cause the value of the local intrinsic rotation velocity. The proper evaluation of the momentum coefficients enables us to evaluate the intrinsic rotation.

8. Summary

The elements determining the V_t profile have been identified, and the roles of these elements on V_t profile are also found. The fast ion losses due to the toroidal field ripple induce CTR rotation in the edge region. As a novel momentum source, this edge localized momentum source has been used for the transient momentum transport analysis. The χ_ϕ and V_{conv} have been separately evaluated using the transient momentum transport analysis. We have found that χ_ϕ, which separated from the convective term increases with increasing χ_i. The $-V_{conv}$ increases with increasing χ_ϕ over a wide range in radii. At low plasma pressure, the steady V_t profiles with CO and CTR-NBIs can be almost reproduced by calculations with χ_ϕ and V_{conv}. On the other hand, At higher plasma pressure, the intrinsic rotation (ΔV_t) increases with increasing $gradP_i$ in CO-, CTR-rotating L-mode plasmas. The results indicate that the local $gradP_i$ appears to cause the local value of intrinsic rotation.

References

[1] Y. Kamada, Plasma Phys. Control. Fusion **42**, A65 (2000).
[2] Special issue on Progress in the ITER Physics Basis [Nucl. Fusion **47**, S18 (2007)].
[3] M. Takechi *et al.,* Phys. Rev. Lett. **98**, 055002 (2007).
[4] H. Reimerdes *et al.,* Phys. Rev. Lett. **98**, 055001 (2007).
[5] Y. Sakamoto *et al.,* Nucl. Fusion **41**, 865 (2001).
[6] E. J. Synakowski *et al.,* Nucl. Fusion **39**, 1733 (1993).
[7] M. Yoshida *et al.,* Plasma Phys. Control. Fusion **48**, 1673 (2006).
[8] W.D. Lee *et al.,* Phys. Rev. Lett. **91**, 205003 (2003).
[9] J. E. Rice *et al.,* in *Proceedings of the 21st IAEA Fusion Energy Conference,* (IAEA, China, 2006) EX/P3-12.
[10] A. Bortolon *et al.,* Phys. Rev. Lett. **97**, 235003 (2006).
[11] K. Ida *et al.,* J. Phys. Soc. Jap. **67**, 4089 (1998).
[12] M. Yoshida *et al.,* Nucl. Fusion **47**, 856 (2007).
[13] O. D Gurcan, P. H. Diamond, T. S. Hahm, *et al.,* Phys. Plasmas **14**, 042306 (2007).
[14] T. S Hahm, P. H. Diamond, O. D Gurcan and G. Rewoldt, Phys. Plasmas **14**, 072302 (2007).
[15] B. Coppi, Nucl. Fusion **42**, 1 (2002).
[16] K. Shinohara *et al.,* Plasma Fusion Res. **1**, 007 (2006).
[17] S. Ide and the JT-60 Team, Nucl. Fusion **45**, S48 (2005).
[18] Y. Koide *et al.,* Phys. Rev. Lett. **72**, 3662 (1994).
[19] H. Shirai *et al.,* in Plasma Physics and Controlled Nuclear Fusion Research 1994 (*Proc. 15th Int. Conf. Seville, 1994*), Vol. 1, p. 355, IAEA, Vienna (1995).